Orientation of shear bands for a rigid plastic frictional material in simple shear

Aurélie Papon, Xiaoxing Liu, Hans Muhlhaus, Lutz Gross

▶ **To cite this version:**

Aurélie Papon, Xiaoxing Liu, Hans Muhlhaus, Lutz Gross. Orientation of shear bands for a rigid plastic frictional material in simple shear. Philosophical Magazine, 2012, Instabilities Across the Scales III, 92 (28-30), pp.3564-3588. 10.1080/14786435.2012.704417 . hal-01736233v2

HAL Id: hal-01736233

https://insa-toulouse.hal.science/hal-01736233v2

Submitted on 7 Sep 2018

HAL is a multi-disciplinary open access archive for the deposit and dissemination of scientific research documents, whether they are published or not. The documents may come from teaching and research institutions in France or abroad, or from public or private research centers.

L'archive ouverte pluridisciplinaire **HAL**, est destinée au dépôt et à la diffusion de documents scientifiques de niveau recherche, publiés ou non, émanant des établissements d'enseignement et de recherche français ou étrangers, des laboratoires publics ou privés.

Orientation of shear bands for a rigid plastic frictional material in simple shear

A. Papon[1], X. Liu[2], H. Muhlhaus[3], L. Gross[4]

[1] *The University of Queensland, Earth Systems Science Computational Centre (ESSCC), School of Earth Sciences, St Lucia, QLD 4072, Australia*

a.papon@uq.edu.au

tel: (+ 61 7) 3346 4089 fax: (+ 61 7) 3346 4134

Corresponding author

[2] *The University of Queensland, Earth Systems Science Computational Centre (ESSCC), School of Earth Sciences, St Lucia, QLD 4072, Australia*

x.liu18@uq.edu.au

tel: (+ 61 7) 3346 4089 fax: (+ 61 7) 3346 4134

[3] *The University of Queensland, Earth Systems Science Computational Centre (ESSCC), School of Earth Sciences, St Lucia, QLD 4072, Australia*

h.muhlhaus@uq.edu.au

tel: (+ 61 7) 3346 4076 fax: (+ 61 7) 3346 4134

[4] *The University of Queensland, Earth Systems Science Computational Centre (ESSCC), School of Earth Sciences, St Lucia, QLD 4072, Australia*

l.gross@uq.edu.au

tel: (+ 61 7) 3346 4114 fax: (+ 61 7) 3346 4134

Orientation of shear bands for a rigid plastic frictional material in simple shear

The orientation of shear bands is investigated analytically and numerically for a rigid plastic frictional material in simple shear. The model is based on co-axial flow rule, incompressible deformations and a friction factor which depends on the strain history. Since we are focussing on geological timescales, the influence of elasticity is neglected. Firstly a linear stability analysis is performed confirming Rice's 1976 assertion [6] that in the hardening regime bifurcation is possible at every stage. Orientation of shear bands against the less compressive principal axis lies anywhere between the Roscoe and Coulomb angles, namely between $\pi/4+\psi/2$ and $\pi/4+\varphi/2$ where φ and ψ are the mobilised angles of friction and dilatancy respectively (in our study we assume $\psi=0$). The linear stability analysis leaves open the question of which orientation will actually emerge in a boundary value problem which consider all nonlinearities. This question is addressed in a finite element study of simple shear with periodic boundary conditions in the shear direction. Our simulations show temporary inclined shear bands in the hardening regime followed by a persistent horizontal shear band. A sensitivity study with respect to geometric and constitutive parameters indicates that the height of the sample controls the orientation of the inclined shear bands. Finally we extend our analytical and numerical studies to Cosserat plasticity. It turns out that inclined shear bands are suppressed for large values of the internal length R (narrow bands). The case of a standard continuum is gradually recovered for small R (wide bands).

Keywords: finite element method, simple shear, plasticity, shear band, orientation, linear stability analysis, Cosserat theory.

1. Introduction

Localisation of deformation during monotonic loading refers to the spontaneous emergence of one or several narrow layers of intense shearing, called shear bands (also known as shear localisation or strain localisation). Because strain localisation occurs in a large range of materials (concrete, metals, soils, rocks) and may affect the stability of structures, this topic has attracted a significant interest during the past four decades [1, 2].

Following previous developments [3-5], we assume that strain localisation may be seen as a constitutive instability. Since we are focussing on geological timescales, we neglect the influence of elasticity and consider a non associated rigid plastic material. According to Rice [6], localisation is possible for any value of the hardening rate for a rigid plastic model with a smooth yield locus. The conditions for the onset of shear bands as well as their orientations have been studied. For elastoplastic models (e.g. with a Mohr-Coulomb or Drucker-Prager type yield criterion), the orientation of shear bands against the direction of the less compressive principal axis is characterised by three values mentioned in literature:

- Coulomb angle: $\frac{\pi}{4}+\frac{\varphi}{2}$
- Roscoe angle [7]: $\frac{\pi}{4}+\frac{\psi}{2}$
- Intermediate angle (Arthur *et al.* [8], Vardoulakis [9]): $\frac{\pi}{4}+\frac{(\varphi+\psi)}{2}$

where φ and ψ are the mobilised angles of friction and dilatancy respectively. The Coulomb angle corresponds to the maximum stress obliquity plane and the Roscoe angle to the zero-extension direction. The intermediate angle corresponds approximately to the lowest bifurcation point in the stress-strain curve of a hardening elastoplastic model [9, 10]. By allowing the material outside the shear band to unload elastically, Vermeer [11] has shown

that all the orientations between the Roscoe and Coulomb angles are admissible in hardening elastoplastic models. This range is confirmed by experimental results for soils in plane strain compression tests [12, 13], in triaxial tests [14], in torsional shear tests [12] and in simple shear tests [15].

Linear stability analysis has been used in literature to characterize the conditions for the onset of shear bands and their orientations (see e.g. [16, 17]). This method is applied in this paper and its results confirm the previous work of Rice [6] and Vermeer [11]: (1) localisation is possible at any stage of hardening and (2) the orientation can be anywhere between the Roscoe and Coulomb angles. However this analytical approach does not allow us to predict which orientation will actually emerge. Therefore in the second part of the paper we turn to a numerical approach.

Numerical studies concerning the orientation of shear bands for certain constitutive models under certain loadings have been proposed within the framework of the finite element method (e.g. [18]) as well as the discrete element method (e.g. [19]). In this paper we focus on continuum mechanics for geophysical materials. In particular, two papers [17, 20] propose a systematic finite element study of the orientation of the shear bands for incompressible viscous - plastic materials under plane strain compression/extension. Lemiale *et al.* [17] considered a Drucker-Prager type failure criterion with material softening, whereas Kaus [20] introduced a Mohr-Coulomb type failure criterion with ideal plasticity. Note that for incompressible materials, these two failure criteria are identical in two dimensions. Most of the literature focuses on rectilinear deformation of the ground state, whereas simple shear tests are seldom treated. Indeed the homogeneity with respect to stress and strain is not easily guaranteed experimentally [15] and numerically. This paper investigates the sparsely covered case of simple shear.

The constitutive relationship selected does not introduce an internal length scale and therefore suffers from a strong mesh dependency [21] when the governing equations lose ellipticity. To overcome this difficulty, regularization methods have been developed [21] (see also review in [22]). In particular Cosserat continuum mechanics [23] introduces three rotations as additional degrees of freedom for each material point. In the context of a granular material represented as a random assembly of rods with the same radius R, this theory allows Mühlhaus and Vardoulakis [24] to determine the thickness of shear bands as a linear function of R. This result is in agreement with experimental observations. Given the physical meaning that the Cosserat theory provides, we use it to extend our original constitutive model.

The aim of this paper is to study analytically and numerically the orientation of shear bands for a frictional rigid plastic material with strain dependent pressure sensitivity in simple shear. The paper is organised as follows. Section 2 presents the constitutive model. A linear stability analysis in Section 3 provides the orientation of shear bands permitted by the constitutive relationship. Both Sections 2 and 3 consider both a standard and a Cosserat continuum (i.e., a continuum without and with internal length respectively). Sections 4 and 5 present numerical results and compare them to analytical results. Section 4 deals with a standard continuum and Section 5 with a Cosserat continuum. Section 6 concludes the paper.

2. Constitutive relations

2.1 Standard continuum

This section considers a standard continuum, a continuum in which internal length scales of the material are ignored. Note that in a later section we will extend the scope of our study to a continuum in which internal length scales are considered.

Here we assume the well known Drucker-Prager yield criterion:

$$\tau = \mu p \tag{1}$$

where $\tau = \sqrt{\frac{1}{2}\sigma'_{ij}\sigma'_{ij}}$ is the equivalent shear stress, **σ'** is the deviatoric stress tensor, summation over equal indexes is implied, μ is the mobilised factor of friction ($\mu = \sin\varphi$, where φ is the mobilised angle of friction) and *p* is the pressure defined as the opposite of the mean stress.

For the numerical study we require a specific functional form for the mobilised friction factor. The following function fits at least qualitatively most known experimental results for loose and dense sands (loose sand is obtained for *n = 2* and dense sand for *n > 2*):

$$\mu(\gamma) = \mu_\infty n^2 \frac{\gamma + \gamma^2}{(1+n\gamma)^2} + \mu_0 \tag{2}$$

where μ_0, μ_∞ and *n* are constitutive parameters and γ is the equivalent shear strain. Figure 1 shows an illustration of (2) for μ_0 = 0.1, μ_∞ = 0.245 and *n* = 7. The flow rule (3) defines the orientation of the stretching tensor **D** in stress space. Note that **D** consists only in the plastic part, possible elastic and viscous parts are neglected.

$$D_{ij} = \dot{\gamma}\frac{\partial\tau}{\partial\sigma'_{ij}} = \dot{\gamma}\frac{\sigma'_{ij}}{2\tau} \tag{3}$$

where $D_{ij} = (v_{i,j} + v_{j,i})/2$, v_i is the ith component of the velocity, the comma followed by an index denotes the partial derivative with respect to that coordinate and $\dot{\gamma}$ is the equivalent shear strain rate. Note that the dot symbol means a total derivative with respect to a time like loading parameter α. In the simple shear case considered here α is the monotonically increasing displacement, prescribed on the top of the shear layer. The shear strain rate is defined as usual as:

$$\dot{\gamma} = \sqrt{2D_{ij}D_{ij}} \tag{4}$$

In Eulerian formulation, the relation between the equivalent shear strain and the equivalent shear strain rate is defined as follows:

$$\dot{\gamma} = \frac{\partial \gamma}{\partial \alpha} + v_i \cdot \frac{\partial \gamma}{\partial x_i} \tag{5}$$

We follow the practise in geophysics of assuming incompressibility (e.g. [17, 20]) of the deformation i.e., $v_{k,k} = 0$. This assumption restricts the generality of the results somewhat; however from previous shear banding studies related to single phase materials it is well known that a choice of $\psi \neq 0$ does not affect the qualitative features of the shear banding process, except when $\psi = \varphi$. Aside from providing a quantitative description of shear banding, the aim of this paper is to highlight qualitative mechanisms using a reduced number of parameters.

2.2 Non-standard continuum (Cosserat plasticity)

In this subsection, we extend the previous model by introducing additional kinematic and static variables, namely the Cosserat spin tensor $\mathbf{W^c}$ and the couple stress or moment stress tensor **m**. This extended or non-standard continuum formulation allows us to consider the effect of an internal length scale within the framework of a continuum theory. Based on the formulation given by Mühlhaus and Vardoulakis [24], the equivalent shear stress is defined by:

$$\tau = \sqrt{a_1 \sigma'_{(ij)} \sigma'_{(ij)} + a_2 \sigma'_{[ij]} \sigma'_{[ij]} + \frac{a_3}{R^2} m_{ij} m_{ij}} \tag{6}$$

where a_1, a_2 and a_3 are constitutive parameters, R is the internal length (e.g. effective particle

radius), $\sigma'_{(ij)}$ and $\sigma'_{[ij]}$ are the components of symmetric and antisymmetric parts of the deviatoric stress tensor respectively.

The evolutions of the stretching tensor **D**, of the relative spin tensor **W-W^c** and of the rate of the micro-curvature tensor **κ** are determined by the following relationships:

$$D_{ij} = \dot{\gamma} \frac{\partial \tau}{\partial \sigma'_{(ij)}} \tag{7.a}$$

$$W_{ij} - W_{ij}^c = \dot{\gamma} \frac{\partial \tau}{\partial \sigma'_{[ij]}} \tag{7.b}$$

$$\kappa_{ij} = \dot{\gamma} \frac{\partial \tau}{\partial m_{ij}} \tag{7.c}$$

where $W_{ij} = \frac{v_{i,j} - v_{j,i}}{2}$ and $\kappa_{ij} = -\frac{1}{2} \in_{ilk} W^c_{lk,j}$, where $\in$ is the permutation symbol.

Combining the relationships (7.a), (7.b) and (7.c) yields the following relationship between the equivalent strain rate $\dot{\gamma}$ and the kinematic variables **D**, **W-W^c** and **κ**:

$$\dot{\gamma} = \sqrt{\frac{1}{a_1} D_{ij} D_{ij} + \frac{1}{a_2} (W_{ij} - W_{ij}^c)(W_{ij} - W_{ij}^c) + \frac{R^2}{a_3} \kappa_{ij} \kappa_{ij}} \tag{8}$$

3. Linear stability analysis

In the following linear instability analysis we focus on bifurcation or eigen-modes of the shear band type, i.e., modes in which the variables depend on one coordinate only, namely $y = (x_i n_i)$ where n_i is the normal vector of the shear band plane.

3.1 Standard continuum

We consider a plane, semi infinite domain $(x_1 < \infty, x_2)$ subject to simple shear. We consider

an infinitesimal continuation $\delta\mathbf{D}$ of the stretching $\mathbf{D}^0$ in the ground state, thus:

$$[\mathbf{D}] = \begin{bmatrix} \delta D_{11} & D_{12}^0 + \delta D_{12} \\ D_{12}^0 + \delta D_{12} & \delta D_{22} \end{bmatrix} \tag{9}$$

From the flow rule (Eq. 3) and the yield criterion (Eq. 1), we obtain:

$$\sigma'_{ij} = \frac{2\mu(\gamma)p}{\dot{\gamma}} D_{ij} \tag{10}$$

Linearising (10) yields:

$$\delta\sigma'_{ij} = \frac{2\mu_{,\gamma}(\gamma)p}{\dot{\gamma}} D_{ij}\delta\gamma - \frac{2\mu(\gamma)p}{\dot{\gamma}^2} D_{ij}\delta\dot{\gamma} + \frac{2\mu(\gamma)\delta p}{\dot{\gamma}} D_{ij} + \frac{2\mu(\gamma)p}{\dot{\gamma}} \delta D_{ij} \tag{11}$$

The advection term in (5) vanishes for the homogeneous ground states so that material and spatial increments coincide. We consider displacement fields of the form:

$$u(x,\alpha) = u(x) \cdot e^{\omega\alpha} \tag{12}$$

where x is the position vector, α a time-like, monotonically increasing loading parameter and ω the growth coefficient. In the present case α is the shear displacement prescribed at $(x_1 < \infty, x_2 = h)$, where h is the initial width of the shear layer. We obtain:

$$\delta\dot{\gamma} = \omega\delta\gamma \tag{13}$$

The incremental, constitutive relationships read:

$$\begin{aligned} \delta\sigma_{11} &= -\delta p + 2\frac{\mu p}{v_{1,2}}\delta v_{1,1} \\ \delta\sigma_{22} &= -\delta p + 2\frac{\mu p}{v_{1,2}}\delta v_{2,2} \\ \delta\sigma_{12} &= \frac{2}{\omega}\mu_{,\gamma} p\,\delta D_{12} + \mu\delta p \end{aligned} \tag{14}$$

Given the assumption of incompressibility and the plane strain condition, we introduce a stream function ψ defined as:

$$\begin{aligned} \delta v_1 &= \psi_{,2} \\ \delta v_2 &= -\psi_{,1} \end{aligned} \tag{15}$$

Substituting (13)-(15) into the incremental form of the equilibrium conditions:

$$\begin{aligned} \delta\sigma_{11,1} + \delta\sigma_{12,2} &= 0 \\ \delta\sigma_{21,1} + \delta\sigma_{22,2} &= 0 \end{aligned} \tag{16}$$

yields the following equations for $(\delta p, \psi)$:

$$\begin{aligned} -\delta p_{,1} + \mu\delta p_{,2} + 2\frac{\mu p}{v_{1,2}}\psi_{,211} + \frac{1}{\omega}\mu_{,\gamma}\, p(\psi_{,222} - \psi_{,112}) &= 0 \\ \mu\delta p_{,1} - \delta p_{,2} + \frac{1}{\omega}\mu_{,\gamma}\, p(\psi_{,221} - \psi_{,111}) - 2\frac{\mu p}{v_{1,2}}\psi_{,122} &= 0 \end{aligned} \tag{17}$$

By elimination of δp from (17) we obtain:

$$\mu_{,\gamma}\frac{1}{\omega}\psi_{,1111} + \mu_{,\gamma}\frac{1}{\omega}\psi_{,2222} + \left(\frac{4\mu}{v_{1,2}} - 2\mu_{,\gamma}\frac{1}{\omega}\right)\psi_{,1122} - \frac{2\mu^2}{v_{1,2}}\psi_{,2111} - \frac{2\mu^2}{v_{1,2}}\psi_{,1222} = 0 \tag{18}$$

We look for solutions of the form:

$$\psi = F(\sin\phi x_1 + \cos\phi x_2) \tag{19}$$

where ϕ is the orientation of the shear band counted clockwise positive from the x-axis (Fig. 2).

Substitution of (19) into (18) yields the following condition for the formation of shear bands in terms of the growth coefficient ω, the orientation ϕ, the mobilised factor of friction μ and the equivalent shear strain γ:

$$\frac{\omega}{v_{1,2}} = \frac{\cos^2 2\phi}{\mu \sin 2\phi(\mu - \sin 2\phi)} \mu_{,\gamma} \qquad (20)$$

Every quadruplet which satisfies this relation corresponds to a permissible shear band. This result is in agreement with Rice's statement in [6] mentioned in the introduction. There are no restrictions on the magnitude of the growth coefficient ω for infinite domains. In this case the most critical band orientation would correspond to the one maximising ω. For $\mu_{,\gamma} > 0$ asymptotic boundary maxima (see Eq. 20) are obtained for $\phi = 0[\pi/2]$ and $\phi = \varphi/2[\pi/2]$; in the latter case we have employed the relationship $\mu = \sin\varphi$. The two orientations correspond to the well known Roscoe and Coulomb orientations respectively.

Figure 3 represents the ratio $\frac{\omega}{v_{1,2}}$ as a function of ϕ for three different values of the equivalent shear strain γ. The vertical asymptotes correspond to the Roscoe and Coulomb angles. For the parameters selected (μ_0 = 0.1, μ_∞ = 0.245 and n = 7), the mobilised friction factor $\mu(\gamma)$ reaches its peak at γ = 0.2. We observe a clear distinction between the curves corresponding to the pre- and post-peak range: before the peak, the angles between the Roscoe and Coulomb angles lead to positive (finite) values of $\frac{\omega}{v_{1,2}}$ and therefore are admissible in the sense that the corresponding mode will grow, whereas after the peak, the angles between the Roscoe and Coulomb angles lead to negative (finite) values of $\frac{\omega}{v_{1,2}}$ and therefore are not admissible. The analytical development presented here refers to an infinite domain, whereas in the numerical simulations in Section 4 we consider a finite domain with $v_1(x_1, x_2 = h)$ prescribed. This boundary condition imposes a constraint on the growth coefficient; we must have $\omega < \infty$. In this case the Roscoe and Coulomb solutions are only admissible for $\mu_{,\gamma} = 0$, i.e., at the peak or for $\gamma \to \infty$. For finite $\omega / v_{1,2}$ we re-write (20) as:

$$\frac{\mu_{,\gamma}}{\mu} = \frac{\sin 2\phi(\mu - \sin 2\phi)}{\cos^2 2\phi} \frac{\omega}{v_{1,2}} \tag{21}$$

Assuming that $\omega / v_{1,2}$ is finite and constant it is reasonable to assume that a band with an orientation maximising $\mu_{,\gamma} / \mu$ will appear first in the loading history. Since (20) has a minimum at $\phi = \varphi / 4$ for φ << 1, (21) has a maximum at the same value, namely at $\phi = \varphi / 4$. This orientation corresponds to the so called intermediate shear band angle, attributed to Vardoulakis [9]. Since the linear instability analyses contain many simplifying assumptions, even for the onset of the localisation process from a homogeneous ground state, it is not clear which band orientation will eventually emerge and persist. This question will be addressed in a numerical study in Section 4.

3.2 Cosserat continuum

Proceeding as in the previous section, we consider the following continuation of the deformation from the ground state:

$$\begin{aligned}
\left[\mathbf{D}\right] &= \begin{bmatrix} \delta D_{11} & D_{12}^0 + \delta D_{12} \\ D_{12}^0 + \delta D_{12} & \delta D_{22} \end{bmatrix} \\
\left[\mathbf{W} - \mathbf{W^c}\right] &= \begin{bmatrix} \delta W_{11} - \delta W_{11}^c & \delta W_{12} - \delta W_{12}^c \\ -\delta W_{12} + \delta W_{12}^c & \delta W_{22} - \delta W_{22}^c \end{bmatrix} \\
\left[\boldsymbol{\kappa}_3\right] &= \begin{bmatrix} \delta \kappa_{31} \\ \delta \kappa_{32} \end{bmatrix}
\end{aligned} \tag{22}$$

From the flow rules (Eq. 7) and the yield criterion (Eq. 1), we obtain the following relationships:

$$\sigma'_{(ij)} = \frac{\mu(\gamma)\, p}{a_1 \dot{\gamma}} D_{ij}$$

$$\sigma'_{[ij]} = \frac{\mu(\gamma)\, p}{a_2 \dot{\gamma}} (W_{ij} - W_{ij}^c) \tag{23}$$

$$m_{3i} = \frac{\mu(\gamma)\, pR^2}{a_3 \dot{\gamma}} \kappa_{3i}$$

Linearising (23) yields:

$$\delta\sigma'_{(ij)} = \frac{\mu_{,\gamma}\, p}{a_1 \dot{\gamma}} D_{ij} \delta\gamma - \frac{\mu p}{a_1 \dot{\gamma}^2} D_{ij} \delta\dot{\gamma} + \frac{\mu \delta p}{a_1 \dot{\gamma}} D_{ij} + \frac{\mu p}{a_1 \dot{\gamma}} \delta D_{ij}$$

$$\delta\sigma'_{[ij]} = \frac{\mu_{,\gamma}\, p}{a_2 \dot{\gamma}} \delta\gamma (W_{ij} - W_{ij}^c) - \frac{\mu p}{a_2 \dot{\gamma}^2} \delta\dot{\gamma} (W_{ij} - W_{ij}^c) + \frac{\mu \delta p}{a_2 \dot{\gamma}} (W_{ij} - W_{ij}^c) + \frac{\mu p}{a_2 \dot{\gamma}} (\delta W_{ij} - \delta W_{ij}^c) \tag{24}$$

$$\delta m_{3i} = \frac{\mu_{,\gamma}\, pR^2}{a_3 \dot{\gamma}} \kappa_{3i} \delta\gamma - \frac{\mu p R^2}{a_3 \dot{\gamma}^2} \kappa_{3i} \delta\dot{\gamma} + \frac{\mu \delta p R^2}{a_3 \dot{\gamma}} \kappa_{3i} + \frac{\mu p R^2}{a_3 \dot{\gamma}} \delta\kappa_{3i}$$

Under the conditions of simple shear (24) reduces to:

$$\delta\sigma_{11} = -\delta p + \frac{\mu p}{a_1 v_{1,2}} \delta v_{1,1} \; ; \delta\sigma_{22} = -\delta p + \frac{\mu p}{a_1 v_{1,2}} \delta v_{2,2} \; ; \; \delta\sigma_{(12)} = \frac{1}{a_1 \omega} \mu_{,\gamma}\, p \delta D_{12} + \frac{\mu}{2 a_1} \delta p$$

$$\delta\sigma_{[12]} = \frac{1}{a_2} \frac{\mu p}{v_{1,2}} (\delta W_{12} - \delta W_{12}^c) \tag{25}$$

$$\delta m_{3i} = \frac{R^2}{a_3} \frac{\mu p}{v_{1,2}} \delta W_{21,i}^c$$

Within the framework of the Cosserat theory, three incremental equations of equilibrium have to be considered in a two-dimensional problem.

$$\begin{aligned} &\delta\sigma_{11,1} + \delta\sigma_{12,2} = 0 \\ &\delta\sigma_{21,1} + \delta\sigma_{22,2} = 0 \\ &\delta m_{31,1} + \delta m_{32,2} + \delta\sigma_{21} - \delta\sigma_{12} = 0 \end{aligned} \tag{26}$$

As in the previous subsection, we introduce a stream function ψ. By restricting our development to small values of a_2 (equivalent to a high Cosserat viscosity, cp. (25)), we may assume the validity of a so-called constrained Cosserat continuum (e.g. [25-26]) for simplicity. In this case:

$$\delta W_{21}^{c} = \delta W_{21} = -\frac{1}{2}(\psi_{,11} + \psi_{,22}) \tag{27}$$

Insertion of (25) and (27) into (26) yields:

$$\begin{aligned} &\frac{1}{a_1}\left(\frac{2\mu}{v_{1,2}} - \frac{1}{\omega}\mu_{,\gamma}\right)\psi_{,2211} + \frac{1}{2a_1\omega}\mu_{,\gamma}(\psi_{,2222} + \psi_{,1111}) - \frac{\mu^2}{2a_1^2 v_{1,2}}(\psi_{,1222} + \psi_{,2111}) + \\ &\frac{R^2}{4a_3}\frac{\mu}{v_{1,2}}\left(\frac{\mu}{a_1}(\psi_{,111121} + 2\psi_{,112221} + \psi_{,222221}) - 3(\psi_{,111122} + \psi_{,112222}) - (\psi_{,222222} + \psi_{,111111})\right) = 0 \end{aligned} \tag{28}$$

By insertion of solutions of type (19) the equation of motion (28) reduces to:

$$\begin{aligned} &F^{(VI)} + \lambda^2 F^{(IV)} = 0 \\ &\lambda^2 = \frac{\frac{1}{2a_1\omega}\mu_{,\gamma}\cos^2 2\phi + \frac{\mu}{2a_1 v_{1,2}}\sin^2 2\phi - \frac{\mu^2}{4a_1^2 v_{1,2}}\sin 2\phi}{\frac{R^2\mu}{4a_3 v_{1,2}}\left(\frac{\mu}{2a_1}\sin 2\phi - 1\right)} \end{aligned} \tag{29}$$

where the super script in roman numeral denotes the order of the derivative with respect to $y = (n_1 x_1 + n_2 x_2)$.

We are interested in periodic solutions, thus λ^2 must be strictly positive. In analogy to the situation in a standard continuum, we choose $a_1 = \frac{1}{2}$ and $a_3 > 0$. The condition $\lambda^2 > 0$ implies:

$$\frac{1}{\omega}\mu_{,\gamma}\cos^2 2\phi + \frac{\mu \sin 2\phi}{v_{1,2}}(\sin 2\phi - \mu) < 0 \tag{30}$$

Assuming $0 \le \phi \le \left(\sin^{-1}\mu\right)/2$, we obtain the following three cases:

$$\text{If } \mu_{,\gamma} > 0\,,\ \frac{\omega}{\nu_{1,2}} > \frac{\cos^2 2\phi}{\mu \sin 2\phi(\mu - \sin 2\phi)}\mu_{,\gamma} \tag{31.a}$$

$$\text{If } \mu_{,\gamma} < 0\,,\ \frac{\nu_{1,2}}{\omega} > \frac{\mu \sin 2\phi(\mu - \sin 2\phi)}{\mu_{,\gamma}\cos^2 2\phi} \tag{31.b}$$

$$\text{If } \mu_{,\gamma} = 0\,,\ \frac{\mu \sin 2\phi}{\nu_{1,2}}(\sin 2\phi - \mu) < 0 \tag{31.c}$$

Equation (31.b) and Equation (31.c) are automatically satisfied if we assume that the orientation angle ϕ remains between the Roscoe and Coulomb angles. Equation (31.a) indicates that if the bifurcation occurs in the hardening regime, then the growth coefficient ω is higher than it would be in a standard continuum. This observation is consistent with Mühlhaus and Vardoulakis [24] concluding that "localisation of the deformation into a shear band is evolving at states beyond the bifurcation state of the classical theory".

In the following section we investigate the fully non-linear problem in terms of numerical solutions based on the finite element method.

4. Finite element simulations, standard continuum

4.1 The numerical model

The simulations are performed with the FEM software Escript [27]. Figure 2 depicts the domain investigated as well as the boundary conditions. For sake of clarity, the mesh is not added to this figure. Note that the mesh is structured (see Table 1 for the reference size of the elements). We assume periodic boundary conditions on the sides which makes the problem somewhat similar to the situation in a torsional shear test with an infinite cell radius. As in the previous sections we assume that the deformation is plane. Here we assume viscous-plasticity

instead of rigid-plasticity. This is implemented by setting a cut-off value for the effective viscosity (hereafter referred to as cut-off viscosity η). Our constitutive relationship then reads:

$$\sigma_{ij} = -p\delta_{ij} + 2\eta_{eff} D_{ij} \tag{32}$$

where $\eta_{eff} = \min(\eta, \frac{\mu p}{\dot{\gamma}})$. In Subsection 4.3 we present a sensitivity study with respect to η.

The geometric and constitutive reference parameters are given in Table 1. To facilitate the emergence of inclined shear bands, we introduce an imperfection, i.e., a zone with a viscosity 100 times lower than the cut-off viscosity in the remaining domain. Concerning the size and the location of the heterogeneity, we follow Kaus's recommendations [20], i.e., the imperfection is resolved numerically with 16 elements and it is located sufficiently far from the top boundary (more than 10 times the heterogeneity size). De Borst [28] indicates that by introducing an imperfection in the domain, the bifurcation problem is transformed into a limit problem and therefore: (1) the correct orientation (i.e., the orientation of the un-perturbed problem) may be determined but (2) the equivalent shear strain at the onset of bifurcation cannot be properly estimated. As a result, we focus in the paper on the band orientation and consider carefully the equivalent shear strain at the onset of shear banding.

The numerical resolution of this problem requires some care because of the incompressibility of the material. We adopt an iterative penalty method (e.g. [29]). The penalty factor is chosen 100 times higher than the cut-off viscosity. In a preliminary study, we used bilinear interpolation functions for the velocities and the pressure was approximated by a piecewise constant field. Single point numerical integration was employed for the pressure term as well as the artificial compressibility term in the velocity equation. This method led to sharp shear bands but introduced a significant tolerance sensitivity probably due to a numerical checkerboard instability in the pressure field. That is why in this paper we use so

called macro elements which do not display these instabilities. For macro elements the pressure and velocity are approximated by a polynomial of order 1 but the velocity approximation is based on a one-step global refinement of the elements. Note that in this paper the size of elements refers to the refinement used for the velocity approximation. The non linear problem is solved iteratively by means of a secant method based on the effective viscosity (Eq. 32). We used a secant method because of its relative robustness in connection with problems involving hardening followed by softening as well as plastic loading-viscous unloading. The convergence criterion is based on the $\mathcal{L}^{\infty}$ norm and the error in the velocity field is defined as:

$$\in_{\chi}^{n} = \frac{\left\| \chi^{n} - \chi^{n-1} \right\|_{\infty}}{\left\| \chi^{n} \right\|_{\infty}} \tag{33}$$

where χ^{n} means the velocity at the iteration *n* and $\left\| \bullet \right\|_{\infty}$ the maximum value of the absolute value over all components and all data points. The convergence tolerance is set to 10^{-4}. Note that in our study, the maximal velocity is prescribed at the top of the domain.

Geometric effects are considered within an Eulerian framework. In the present case the only location in our model where geometric effects need to be considered is in the advection term in (5). Equation (5) is solved using the two-step explicit Taylor-Galerkin method outlined in [30].

A sensitivity study with respect to the size of the incremental loading step was performed and showed that a value of 0.01 is sufficient to reproduce and investigate the salient features of shear bands.

The orientation of the shear bands is measured from a high-resolution plot of the equivalent shear strain rate. The accuracy of the measurement depends on the curvature of the band and therefore on the distance over which the band is a straight line. In the following, the

shear band is considered straight over the reference width of the simulation ($L^{ref} = 4$). The error of measurement is estimated to be equal to ±0.2 degree. Viscous unloading outside the shear bands occurs upon bifurcation. Therefore the width of the shear bands can be characterised without ambiguity by the extent of the plastic zone.

In the following subsection, we present the results given by a simulation based on the reference parameters depicted in Table 1 and analyse the shear bands in terms of orientation, thickness and intensity. Note that given the periodic boundary conditions and assuming that the band orientation is constant throughout the domain, a straightforward geometrical relation can be determined between the orientation of the shear bands, their spacing and the width of the domain. The sensitivity of the results with respect to the parameter values (Table 1) will also be investigated.

4.2 Simulation based on the reference parameters

Figure 4 (a) shows the mean shear stress σ_{12} as a function of the mean equivalent shear strain. The mean variables refer to the variables at the location ($x_1 = 0.2$; $x_2 = 0.5$). By considering this location, the difference between the simulations with and without imperfection is not significant before the first bifurcation. Figure 4 (b-d) represents the equivalent shear strain rate at three stages of the simulation. The first stage (Fig. 4 (b)) corresponds to pre-bifurcation, in which the simple shear ground state dominates. The spatial distribution of the variables is quasi-homogeneous and the velocity profile along a cross-section (Fig. 5) is almost linear. The second stage (Fig. 4(c)) starts with the emergence of two sets of shear bands. The first set of shear bands consists of two horizontal shear bands at the bottom and top of the domain. The second set corresponds to inclined shear bands whose orientation angles are different from zero and smaller than 45 degrees. The velocity profile in Figure 5 highlights the alternation between plasticised zones (second set of shear bands) and the viscous quasi-rigid

unloaded zones. Finally the third stage (Fig. 4(d)) is characterized by a significant decrease of the shear stress and a high value of the equivalent shear strain ($\dot{\gamma} > 16$) within a horizontal shear band. The inclined shear bands have disappeared. Consequently the velocity profile shows a quasi-rigid zone and a highly sheared zone (Fig. 5). Note that the persistent horizontal shear band extends over two elements (Fig. 4(d)). This is due to the use of different meshes for the pressure and the velocity.

We investigate the orientation of the second set of shear bands at the loading increment following the bifurcation. We measure an angle of 4.5 degrees (Fig. 4(c)) and compare it to the classical values given in the literature: 0 degree (Roscoe angle), 8.3 degrees (intermediate angle) and 16.6 degrees (Coulomb angle). It appears that the observed angle does not correspond to a particular value. According to the value of the equivalent shear strain at bifurcation (γ_{bif} = 0.092) and the orientation of the shear band, the value of the ratio $\frac{\omega}{v_{1,2}}$ is determined (Fig. 6, *h=1*). The ratio is strictly positive so that the angle is permitted by the previous analysis (see Subsection 3.1). The orientation of the persistent horizontal shear band corresponds to the Roscoe angle. However it seems difficult to track analytically the emergence of this shear band since the inclined shear bands modify the ground state and therefore the conditions of the previous analysis are not fulfilled anymore just before the formation of the horizontal shear band.

To confirm the results with respect to mesh dependency, we carry out two additional calculations with a coarse mesh (200 x 50 elements) and a fine mesh (800 x 200 elements). The thickness and the orientation of the shear bands are shown in Figures 7 (a) and (b) respectively. The band orientation remains 4.5 degrees for a fine mesh, but increases to 5.2 degrees for a coarse mesh. The width of the shear bands depends strongly on the mesh size. The widths of the inclined shear bands are equal to 0.11, 0.14 and 0.22 for the fine, reference

and coarse meshes respectively. The persistent shear bands extend over two elements. The stress-strain curves are compared to that of the reference mesh in Figure 7 (c). The results obtained from this mesh sensitivity study are in agreement with the properties of a so-called local model and highlight the numerical difficulties encountered when using this kind of model. Moreover in this study we focus on the orientation of the inclined shear bands. The orientations observed in our study range from around 3 to 8 degrees so that the selected structured mesh does not affect the band orientation by mesh alignment.

In the following sections, we focus on the inclined shear bands. We investigate the influence of the value of the cut-off viscosity and dimensions of the computational domain on band orientation.

4.3 Influence of the cut-off viscosity

Vermeer [11] suggests that the band angle observed in numerical simulations based on elastic – plastic material behaviour is related to the capability of the material to unload, an effect which is beyond the scope of a linear instability analysis. In order to explore the relevance[1] of Vermeer's assertion in the context of viscous – plastic behaviour we perform a sensitivity study with respect to the cut-off viscosity. Note that the viscosity of the weak zone is kept 100 times smaller than the cut-off viscosity and that we restrict our study to cut-off viscosity values high enough to represent a rigid plastic material.

We consider two values for the cut-off viscosity η: 600 and 1200. For these values, the equivalent shear strain at bifurcation is γ_{bif} = 0.092 and 0.1, respectively, compared to γ_{bif} = 0.092 observed in the simulation with η = 800 (Table 1). Therefore, in both simulations,

[1] Elastic and plastic strain rates do not share the same principal axes whereas viscous and plastic strain rates do.

the analytical value of the intermediate angle is about 8.4 degrees. Figure 8 (a-b) shows an orientation of 4.7 and 4.5 degrees for simulations with $\eta = 600$ and 1200, respectively.

Given these observations we may conclude that for rigid plastic material the exact value of the cut-off viscosity does not significantly influence the strain at the onset of bifurcation, nor the orientation of the inclined shear bands.

4.4 Influence of the height of the domain

The geometry parameter *h* corresponding to the height of the domain does not occur in the linear stability analysis firstly, because of the absence of an internal length scale and, secondly, because the boundary conditions at the intersection of the shear band/layer surface at $x_2 = h$ are ignored. Therefore the bifurcation condition (Eq. 20) is independent of *h*. However according to Tatsuoka *et al.* [12] and Desrues *et al.* [13], the orientation of shear bands may depend on the size of the specimen: the higher the specimen, the steeper the shear band. The aim of this subsection is to investigate the influence of the layer height *h* on the bifurcation strain and the band orientation.

In the simulations with dimensionless heights 0.5, 1, 2, 4, the equivalent shear strains at the onset of bifurcation are 0.08, 0.092, 0.112, 0.128 and the intermediate angles are 7.9, 8.3, 8.7, 8.9 degrees respectively. We observe the orientation of the shear band: as height increases, the orientation angle also increases: 2.8, 4.5, 6, 8 degrees (Fig. 6). The difference in the orientations cannot be explained by the difference in the intermediate angles. According to these results, the height of the domain controls the orientation of the inclined shear bands. This suggests that the geometrical conditions act as a filter for the infinite number of admissible orientations mentioned in the analytical study. This filtering can be explained as the result of the rigid plastic conditions studied here. Indeed this behaviour permits very small deformations in the unloading zone.

4.5 Influence of the width of the domain

Given the periodic boundary conditions, we do not expect that the width of the domain can influence the shear band patterns. However, we performed an additional simulation with a width equal to 10. Inclined shear bands appear at the same bifurcation shear strain ($\gamma_{bif} = 0.092$) and with the same orientation (4.5 degrees) as that observed in the simulation with the reference parameters. Therefore the width of the shear layer does not influence the orientation of the inclined shear bands if periodic boundary conditions are assumed.

4.6 Discussion

In this section, we investigated the bifurcation problem from a numerical point of view. We focussed on inclined shear bands formed in the hardening regime. In addition to Equation (20), further constraints such as influences from the boundary conditions and geometry parameters have to be considered to explain the exact morphology of the shear bands. It has been observed that the height of the domain has a significant influence on the band orientation, probably due to the rigid plastic behaviour of the material.

5. Simulations with internal length (Cosserat effects)

In this section, we extend our numerical investigation to an internal length scale R. We describe briefly the numerical scheme used to solve the non linear problem and then present a sensitivity study with respect to the internal length R.

5.1 Computational aspects

The numerical procedure for the Cosserat model mostly follows the one for the standard continuum outlined in Subsection 4.1. In the following we emphasize the differences between the approaches. Figure 2 represents the computational domain as well as the boundary

conditions and Table 1 summarises the parameter values assumed. We couple the momentum (velocity problem) and angular momentum equations (spin problem) iteratively. We start with $W_3^c = 0$. In each iteration, first we solve the velocity problem and update the pressure according to the penalty method, then solve the spin problem. We obtain an update for W_3^c. An outline of the procedure including the steps resulting from the iterative penalty method is represented in Figure 9.

As explained previously, we introduce a weak zone, that is, an imperfection with a cut-off viscosity 100 times smaller than the viscosity in the surrounding domain. Note that the Cosserat viscosity is also reduced since it depends on the cut-off viscosity according to $\eta_c = \frac{\eta}{a_2}$.

5.2 Results

In the following, we focus on the sensitivity of the numerical solution with respect to *R*, since *R* is the key additional parameter introduced by the Cosserat theory. According to Mühlhaus and Vardoulakis [24], the width of the shear bands depends linearly on the parameter *R*. Simulations with different values of *R* are performed. From them, three main observations arise: (1) in all the simulations we observe a progressive unloading from the top to the bottom of the domain, (2) during this unloading inclined shear bands form within the unloading zone in the simulations with R ≤ 0.005 (Fig. 10) and (3) we observe a persistent horizontal shear band at the bottom of the domain, whereas inclined shear bands are not observed.

Figure 11 shows the width of the persistent horizontal shear band as a function of the parameter *R*. For values of *R* between 0.004 and 0.05, the relation is linear, which is in agreement with the conclusions of Mühlhaus and Vardoulakis [24], whereas for values of *R* smaller than 0.004, the linearity is not preserved. In fact, for $R \to 0$, we would expect the

band thickness to reduce to the width of two elements (as observed for standard continuum), which is 0.02 in the present case. Instead we observe a wider band width of approximately 0.06. This discrepancy is a consequence of our choice of interpolation functions for the Cosserat spin W_3^c and the velocities from C^0 continuous bilinear functions. This choice causes a bending effect dependent on the mesh size as shown in Appendix 1. The results obtained from a simulation with a fine mesh (800 x 200 elements) are denoted by a dashed line in Figure 11. For values of R higher than 0.05, boundary effects appear. Indeed an additional simulation with $h = 2$ and $R=0.08$ is performed and the width of the shear band is denoted by dashed line in Figure 11. This result agrees with the linear relation observed for values of R inferior to 0.05. Figures 12 and 13 represent for different values of R the velocity profile and the stress-strain curve, respectively. Note that for $R = 0.05$ the location ($x_1 = 0.2$; $x_2 = 0.5$) at which the equivalent shear strain and the shear stress are observed is inside the shear band.

The inclined shear bands ($R \leq 0.005$) form at the first increment at which unloading occurs and disappear after around 5 steps. The larger the parameter R, the thicker the inclined shear bands. The orientation is around 4.2 degrees for all $R \leq 0.005$ (with variations smaller than the measurement error). These observations may be interpreted as a smooth transition between a standard continuum ($R = 0$) and a Cosserat continuum ($R > 0$).

6. Conclusion

In this paper, a bifurcation problem was investigated analytically and numerically within the framework of a standard as well as a Cosserat continuum. We considered a rigid plastic frictional material in simple shear. More specifically the constitutive model is based on co-axial flow rule, incompressible deformations and a friction factor which depends on the strain history.

The analytical study consisted of two linear stability analyses. The search for hyperbolic solutions led to three main conclusions: (1) the three values given in literature (the Roscoe, Coulomb and intermediate angles) are obtained as special cases from the transcendental condition (Eq. 20), (2) for a standard continuum, bifurcation is permitted in the hardening regime at any value of the accumulated equivalent plastic strain and (3) it occurs at a strain lower than that observed in the Cosserat theory.

For a standard continuum, the simulations show three stages: the quasi-homogeneous state, then the emergence of inclined temporary shear bands whose orientations are between the Roscoe and Coulomb angles, and finally the onset of a persistent horizontal shear band. The width of the shear bands depends strongly on the mesh size, as expected. The sensitivity study shows that the parameter with the most influence on the orientation of the inclined shear bands is the height of the sample. As height increases, the orientation angle also increases. For a Cosserat material we observed a progressive unloading from top to bottom. During this unloading and for $R \leq 0.005$, the unloaded zone is crossed by inclined shear bands. As expected, the width of the persistent shear bands is linear with respect to the internal length R.

By considering analytical and numerical approaches, this paper highlighted the limitations of the analytical study as well as the additional geometrical constraints introduced in the simulations such as the height of the domain and the boundary conditions. The linear stability analysis leads to an infinite number of admissible orientations in the hardening regime. However the "numerical filter" keeps only the most stable solution in terms of the chosen convergence criterion. Under these conditions and for the rigid plastic frictional material studied here, the numerical solution is mainly controlled by geometrical conditions.

Acknowledgement

We would like to acknowledge support from the ARC Discovery Grant DP0985662 and the ongoing support through Auscope/NCRIS. We are also grateful to Cihan Altinay, Joel Fenwick, Lin Gao and

Vince Boros of ESSCC at the University of Queensland for their help during the preparation of the manuscript.

Appendix

For sake of simplicity, we assume a homogeneous linear elastic material in simple shear (see Fig. 2). The problem is treated as a one dimensional problem. Considering the x_1-invariance of the problem, the constitutive relationships are:

$$\begin{aligned} \sigma_{12} &= G u_{1,2} + G^c (u_{1,2} - \omega_3^c) \\ \sigma_{21} &= G u_{1,2} - G^c (u_{1,2} - \omega_3^c) \\ \mu_{32} &= G^c R^2 \omega_{3,2}^c \end{aligned} \tag{A.1}$$

where G and G^c are the shear modulus and the Cosserat shear modulus respectively, **u** the displacement vector and ω^c the Cosserat rotation. The other notations are defined as done in the main part of the paper.

We assume linear interpolation functions for the displacements and the Cosserat rotation:

$$\begin{aligned} \mathbf{u} &= \frac{\mathbf{u}^i + \mathbf{u}^j}{2} + \frac{\mathbf{u}^j - \mathbf{u}^i}{\Delta x_2} x_2 \\ \omega_3^c &= \frac{\omega_3^{c\,i} + \omega_3^{c\,j}}{2} + \frac{\omega_3^{c\,j} - \omega_3^{c\,i}}{\Delta x_2} x_2 \end{aligned} \tag{A.2}$$

where the superscripts i and j denote the nodes of a linear element and $\Delta x_2 = x_2^j - x_2^i$ its length.

Within the framework of the Cosserat theory, the internal virtual work of a linear element reads:

$$\delta W^{\text{int}} = \int_{-\Delta x_2/2}^{\Delta x_2/2} \left(\sigma_{(ij)} \delta \varepsilon_{ij} + \sigma_{[ij]} \left(\delta \omega_{ij} - \delta \omega_3^c \right) + \mu_{ij} \delta k_{ij} \right) dx_2 \tag{A.3}$$

where $\delta \varepsilon_{ij} = \frac{u_{i,j} + u_{j,i}}{2}$, $\delta \omega_{ij} = \frac{u_{i,j} - u_{j,i}}{2}$ and $\delta k_{ij} = \omega_{i,j}^c$ are the components of the virtual strain

tensor, of the virtual macro-curvature tensor and of the virtual micro-curvature tensor respectively.

Substituting of (A.2) into (A.3) yields:

$$\delta W^{\text{int}} = \int_{-\Delta x_2/2}^{\Delta x_2/2} G u_{1,2} \delta u_{1,2} dx_2 + \int_{-\Delta x_2/2}^{\Delta x_2/2} G^c (u_{1,2} - \omega_3^c)(\delta u_{1,2} - \delta \omega_3^c) dx_2 + \int_{-\Delta x_2/2}^{\Delta x_2/2} G^c R^2 \omega_{3,2}^c \delta \omega_{3,2}^c dx_2 \quad \text{(A.4)}$$

Noting that the integration of odd functions evaluates to zero, the virtual internal work can be re-written as:

$$\delta W^{\text{int}} = G\gamma\delta\gamma\Delta x_2 + G^c \left[(\gamma - W)(\delta\gamma - \delta W) + K\delta K \left(\frac{\Delta x_2^2}{12} + R^2 \right) \right] \Delta x_2 \quad \text{(A.5)}$$

where $\gamma = \dfrac{u_1^j - u_1^i}{\Delta x_2}$, $K = \dfrac{\omega_3^{c\,j} - \omega_3^{c\,i}}{\Delta x_2}$ and $W = \dfrac{\omega_3^{c\,j} + \omega_3^{c\,i}}{2}$.

Equation (A.5) shows a bending term which depends not only on the internal length R and but also on the mesh size Δx_2.

References

[1] I. Vardoulakis and J. Sulem, *Bifurcation Analysis In Geomechanics*, Blackie Academic & Professional, Glasgow, 2005.

[2] G. Mandl, *Rock Joints The Mechanical Genesis*, Springer, Berlin, 2005.

[3] R. Hill, J. Mech. Phys. Solids 1 (1952) p.19.

[4] J. Mandel, *Conditions de stabilité et postulat de Drucker* in *Proc. IUTAM Symp. on Rheology and Soil Mechanics*, J. Kravtchenko and P. M. Sirieys, eds., Springer, Berlin, 1966, p.58.

[5] J. W. Rudnicki and J. R. Rice, J. Mech. Phys. Solids 23 (1975) p.371.

[6] J. R. Rice, *The localization of plastic deformation* in *Proc. of the 14th International Congress on Theoretical and Applied Mechanics,* W. T. Koiter, ed., North Holland Publishing Co., Amsterdam, 1976, p.207.

[7] K. H. Roscoe, Géotechnique 20 (1970) p.129.

[8] J. R. F. Arthur, T. Dunstan, Q. A. J. L. Al-Ani and A. Assadi, Géotechnique 27 (1977) p.53.

[9] I. Vardoulakis, Int. J. Numer. Anal. Meth. Geomech. 4 (1980) p.103.

[10] P. A. Vermeer, *A simple shear-band analysis using compliances*, in *Proc. IUTAM Symp. Deformation and Failure of Granular Materials*, P. A. Vermeer and H. J. Luger, eds., Balkema, Rotterdam, 1982, p.493.

[11] P. A. Vermeer, Géotechnique 40 (1990) p.223.

[12] F. Tatsuoka, S. Nakamura, C.-C. Huang and K. Tani, Soils Found. 30 (1990) p.35.

[13] J. Desrues and G. Viggiani, Int. J. Numer. Anal. Meth. Geomech. 28 (2004) p.279.

[14] P. Bésuelle, J. Desrues and S. Raynaud, Int. J. Rock Mech. Min. 37 (2000), p.1223.

[15] M. Budhu, Can. Geotech. J. 25 (1988) p.395.

[16] A. Needleman, J. Mech. Phys. Solids 27 (1979) p.231.

[17] V. Lemiale, H.-B. Mühlhaus, L. Moresi and J. Stafford, Phys. Earth Planet. Inter. 171 (2008) p.177.

[18] J. H. Prevost and T. J. R. Hughes, J. Appl. Mech. 48 (1981) p.69.

[19] J. P. Bardet and J. Proubet, J. Eng. Mech-ASCE 118 (1992) p. 397.

[20] B. J. P. Kaus, Tectonophysics 484 (2010) p.36.

[21] R. de Borst, L.J. Sluys, H-.B. Mühlhaus and J. Pamin, Eng. Computation 10 (1993) p.99.

[22] J. Tejchman and W. Wu, Acta Mech. 99 (1993) p.61.

[23] E. Cosserat and F. Cosserat, *Théorie des Corps Déformables*, Hermann et fils, Paris, 1909.

[24] H.-B. Mühlhaus and I. Vardoulakis, Géotechnique 37 (1987) p.271.

[25] R.D. Mindlin and H.F. Thiersten, Effects of Couple-stresses in Linear Elasticity, Arch. Ration. Mech. An. 11 (1962) p. 415.

[26] N.A. Fleck and J.W. Hutchinson, Adv. Appl. Mech. 33 (1997) p. 295.

[27] L. Gross, L. Bourgouin, A. J. Hale and H.-B Muhlhaus, Phys. Earth Planet. Inter. 163 (2007) p.23.

[28] R. de Borst, Int. J. Numer. Anal. Meth. Geomech. 12 (1988) p.99.

[29] O.C. Zienkiewicz and R.L. Taylor, *The Finite Element Method*, 5th ed., Vol.1, Butterworth-Heinemann, Oxford, 2000.

[30] B. Roig, J. Comput. Appl. Math. 204 (2007) p. 95.

Figures

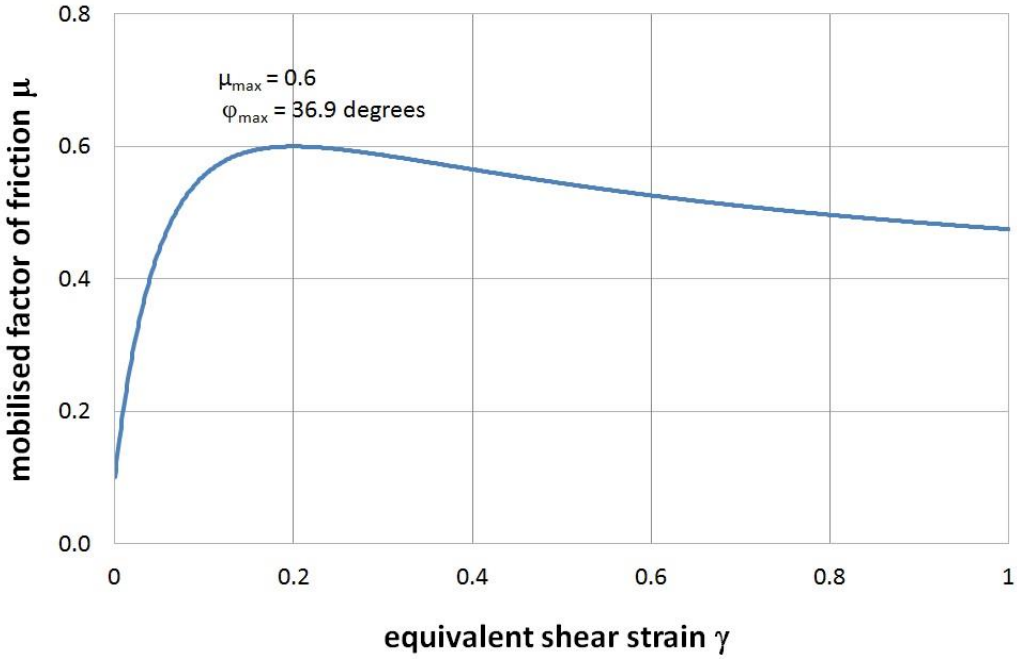

Figure 1: Evolution of the mobilised factor of friction μ as a function of the equivalent shear strain γ.

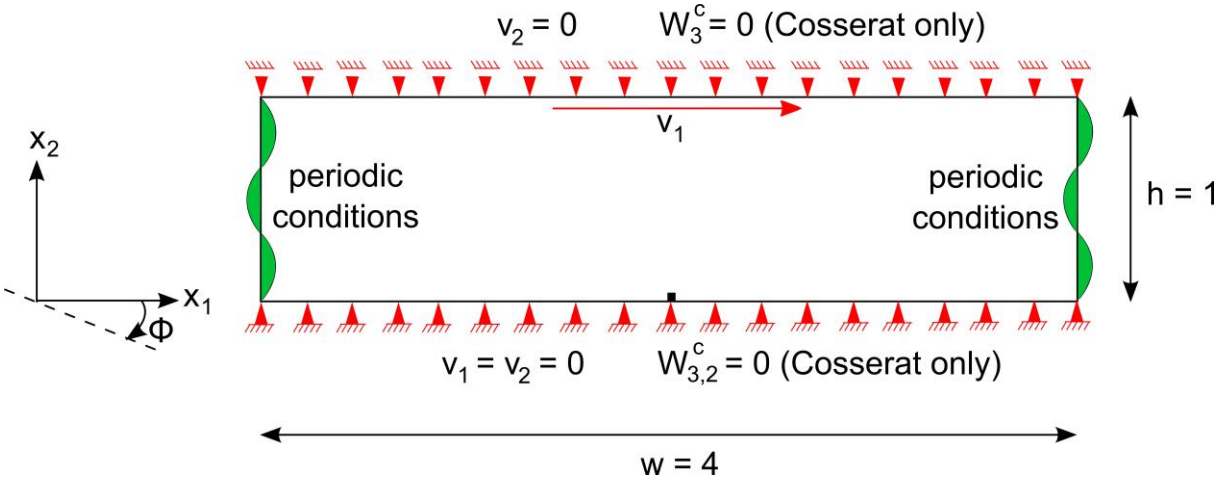

Figure 2: Rectangular specimen in simple shear.

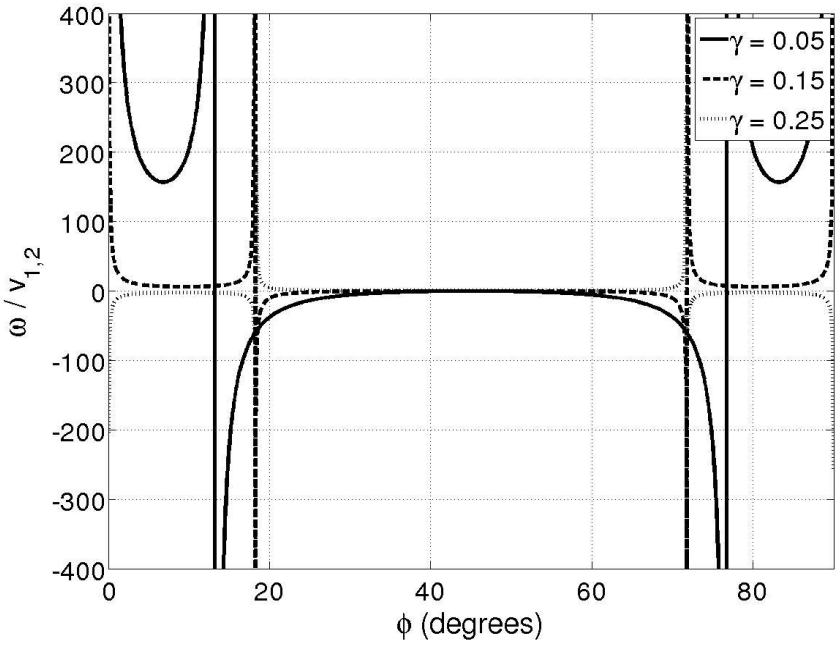

Figure 3: Bifurcation condition within the framework of standard mechanics for different values of the equivalent shear strain (see Eq. 20).

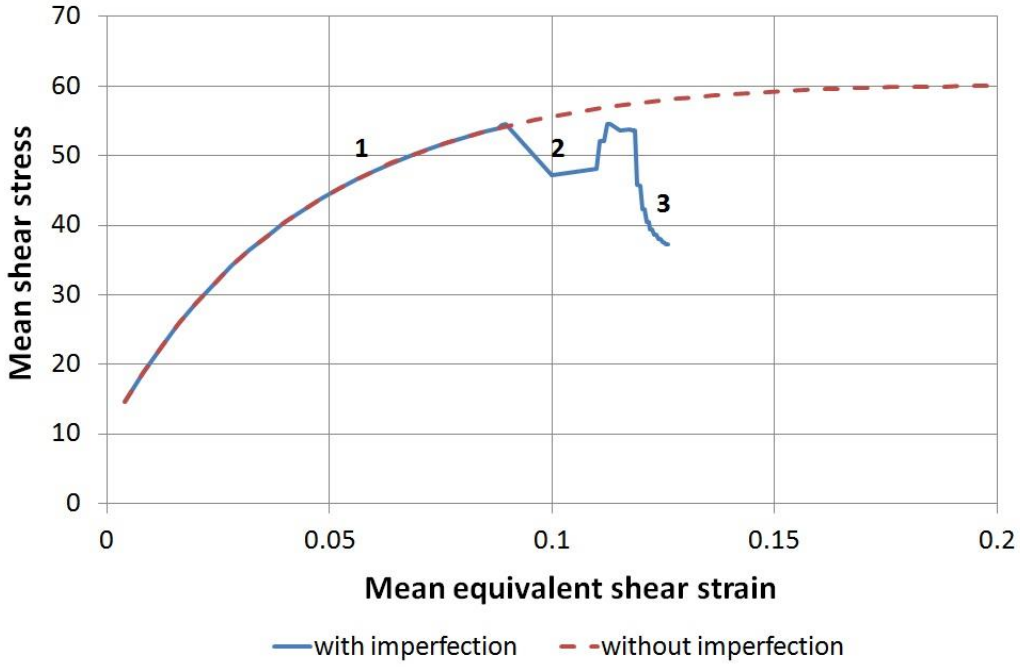

Figure 4a: Three stages during the simulation with the reference parameters highlighted in the stress-strain curve.

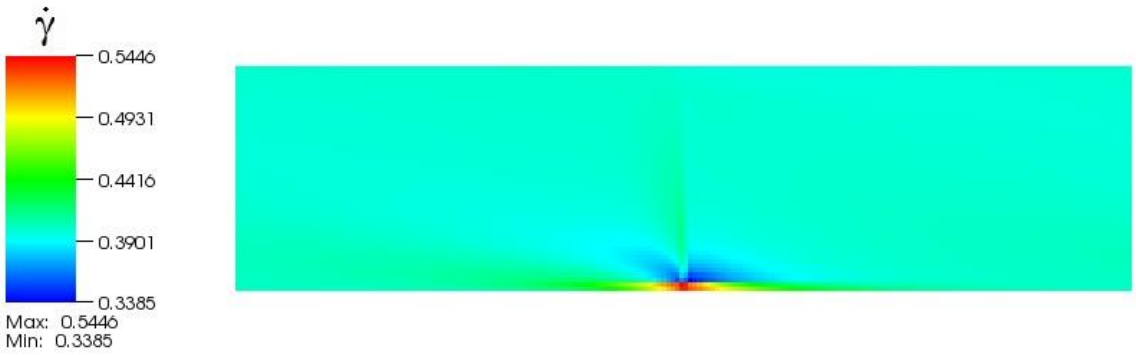

Figure 4b: Stage 1: quasi-homogeneous state.

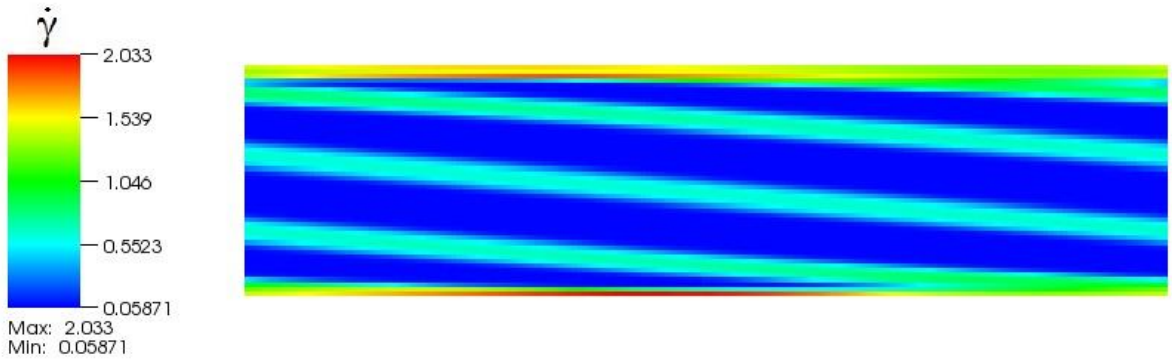

Figure 4c: Stage 2: inclined shear bands with two shear bands at the bottom and at the top of the domain.

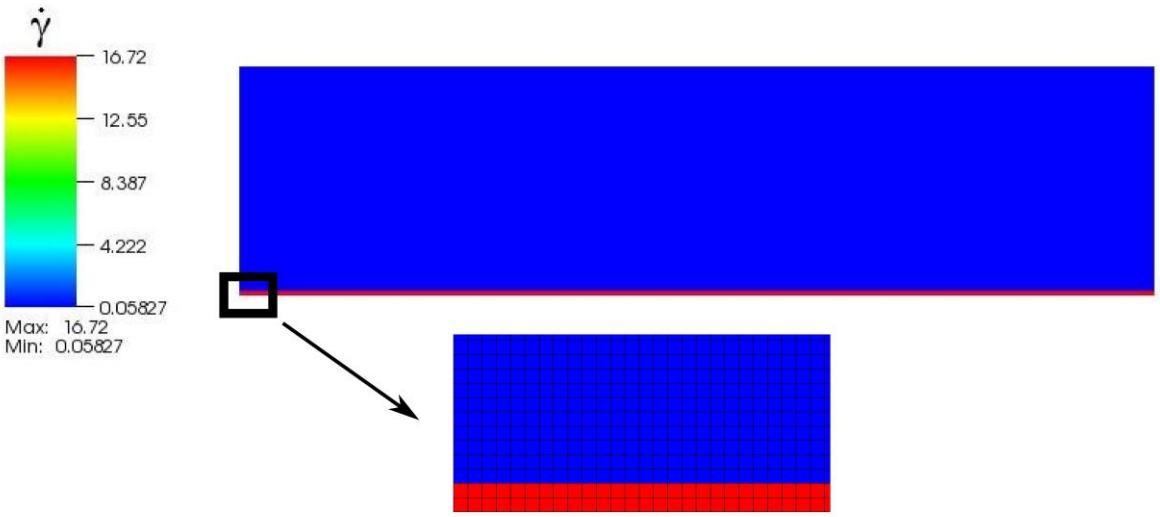

Figure 4d: Stage 3: persistent horizontal shear band at the bottom of the domain.

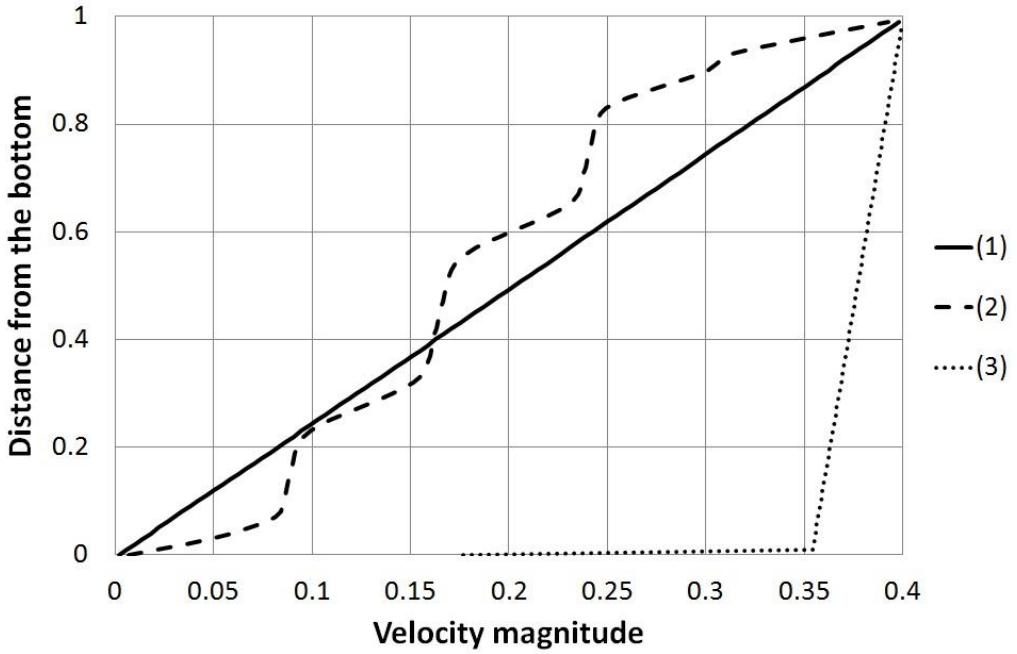

Figure 5: Velocity profile along a cross section for the three different stages observed during the simulation with the reference parameters.

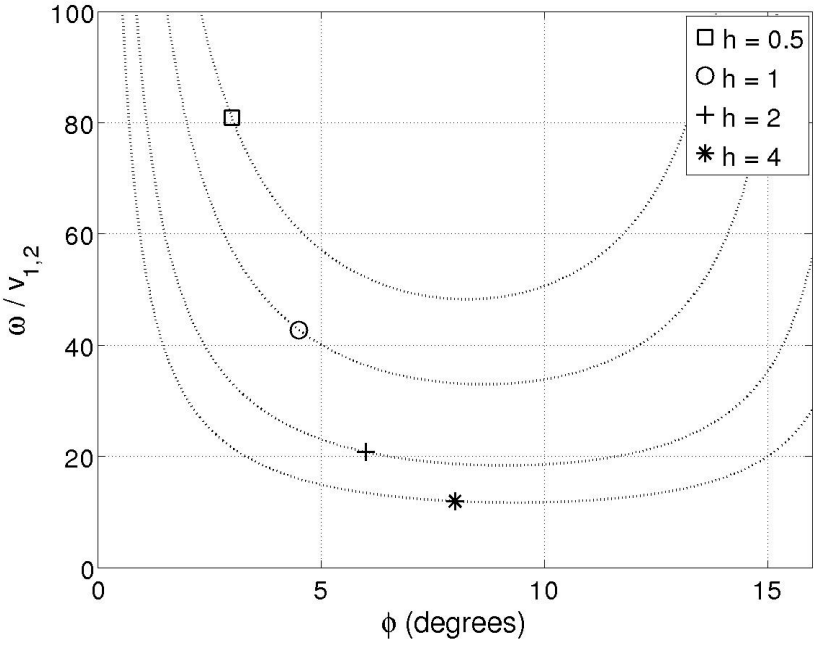

Figure 6: Bifurcation point for different values of *h* in the space $\phi - \frac{\omega}{v_{1,2}}$.

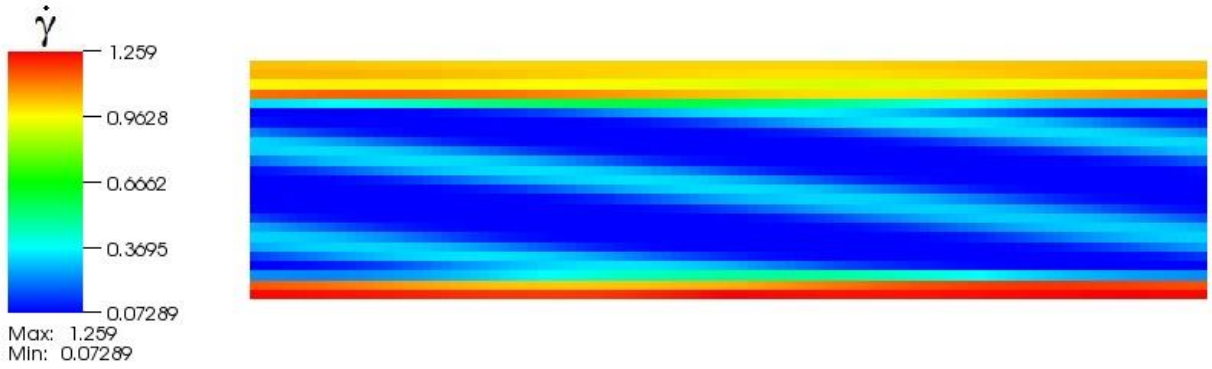

Figure 7a: For a coarse mesh (200 x 50 elements): band orientation and thickness.

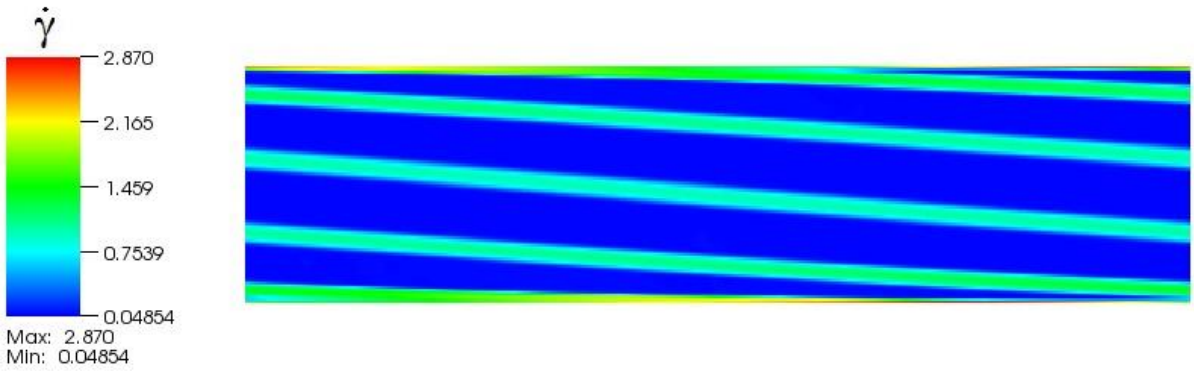

Figure 7b: For a fine mesh (800 x 200 elements): band orientation and thickness.

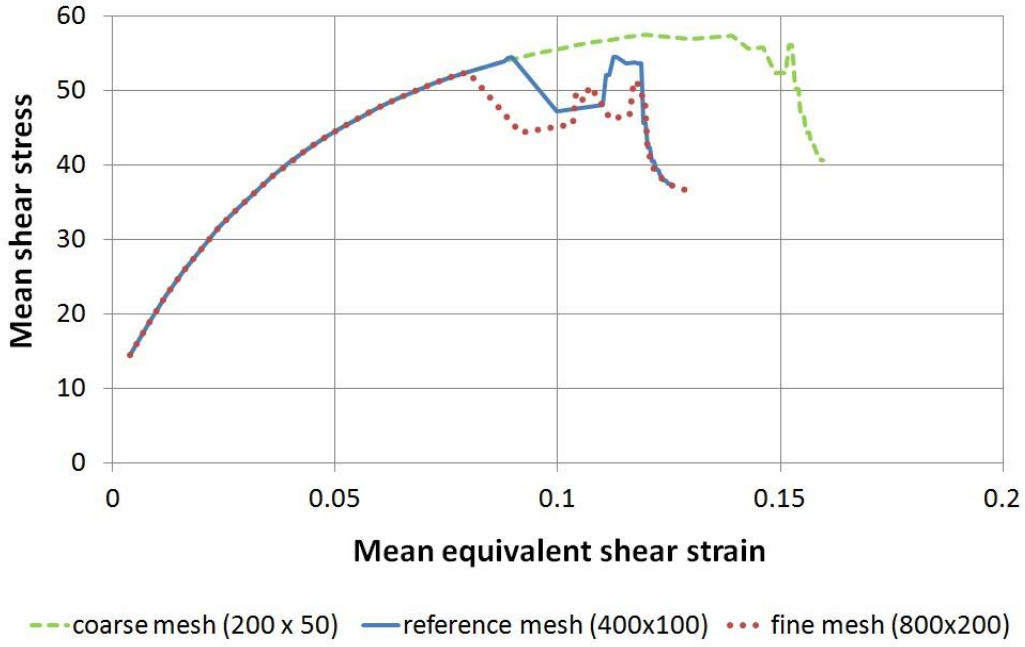

Figure 7c: Stress-strain curves for a fine mesh (800 x 200 elements) and a coarse mesh (200 x 50 elements).

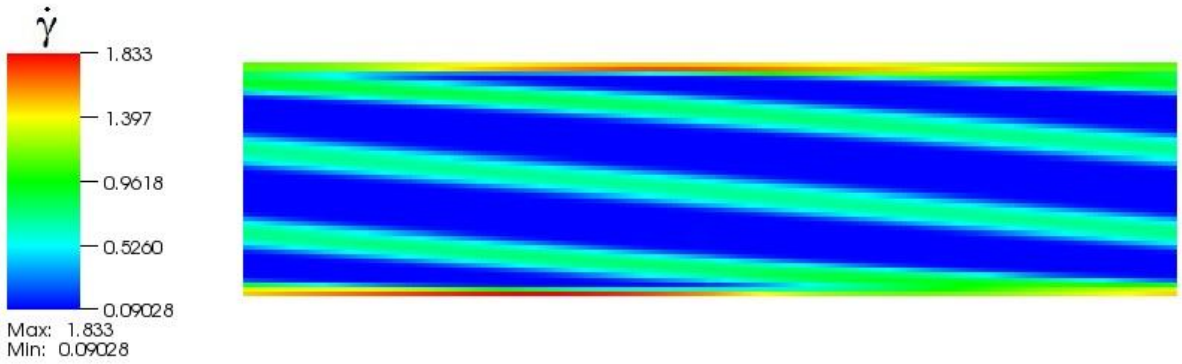

Figure 8a: Band orientation for $\eta = 600$.

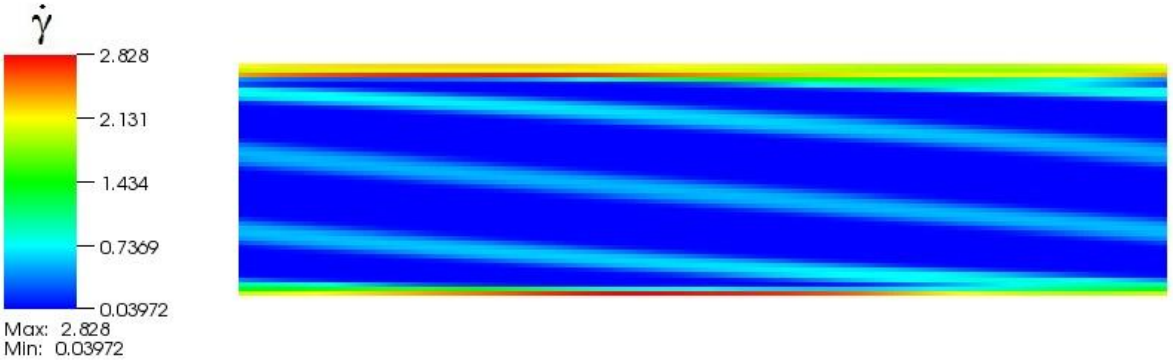

Figure 8b: Band orientation for η = 1200.

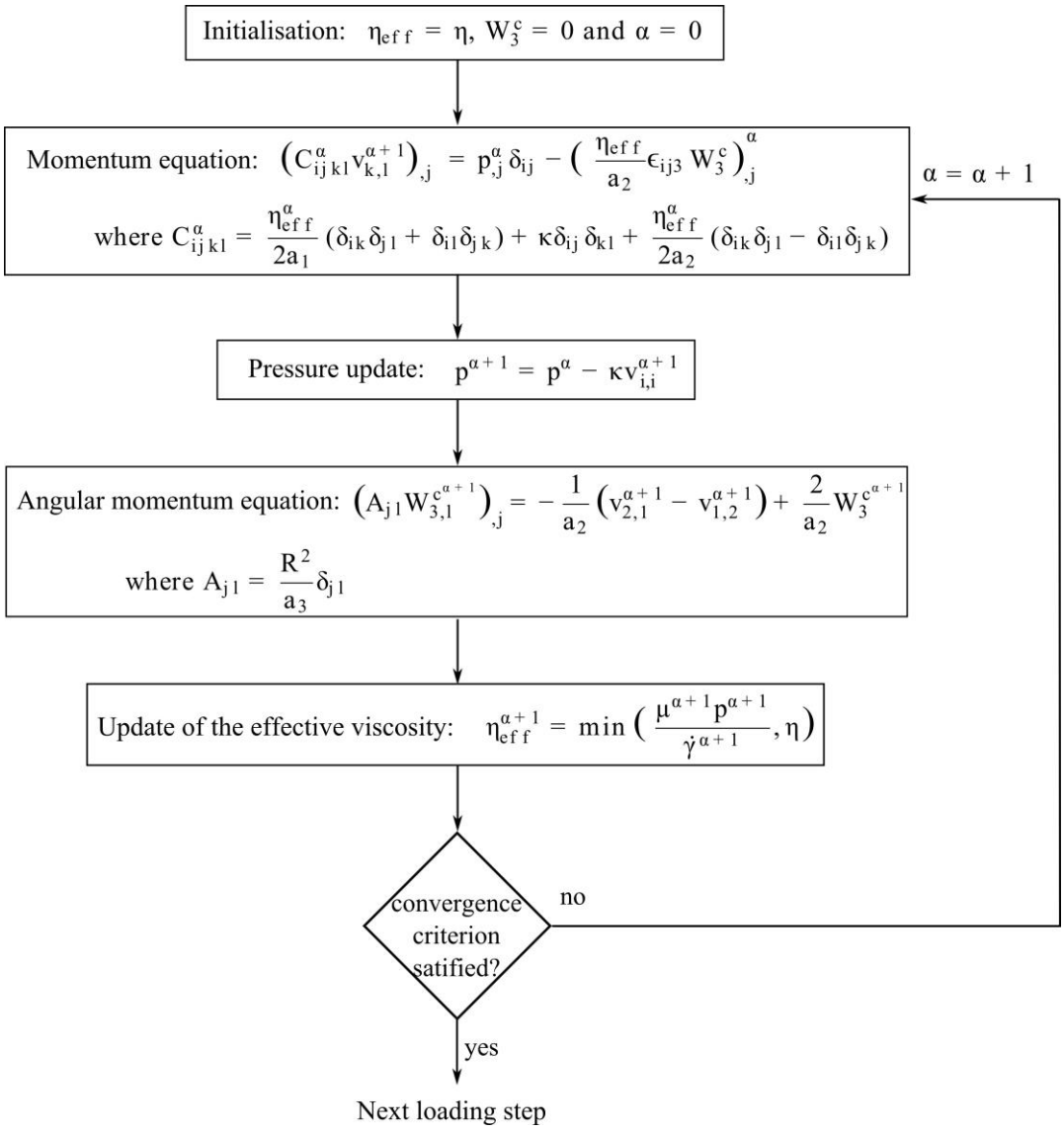

Figure 9: Flow chart of the procedure for Cosserat plasticity.

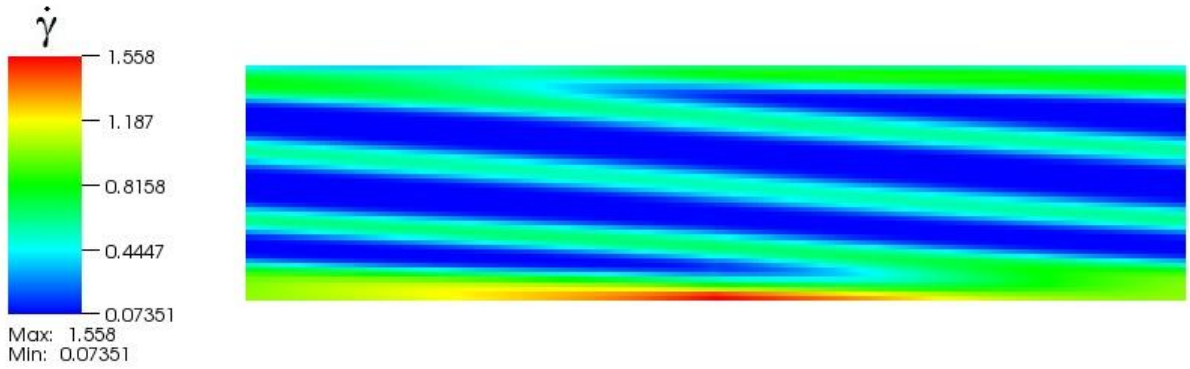

Figure 10: Distribution of the equivalent shear strain rate showing inclined shear bands for $R = 0.001$.

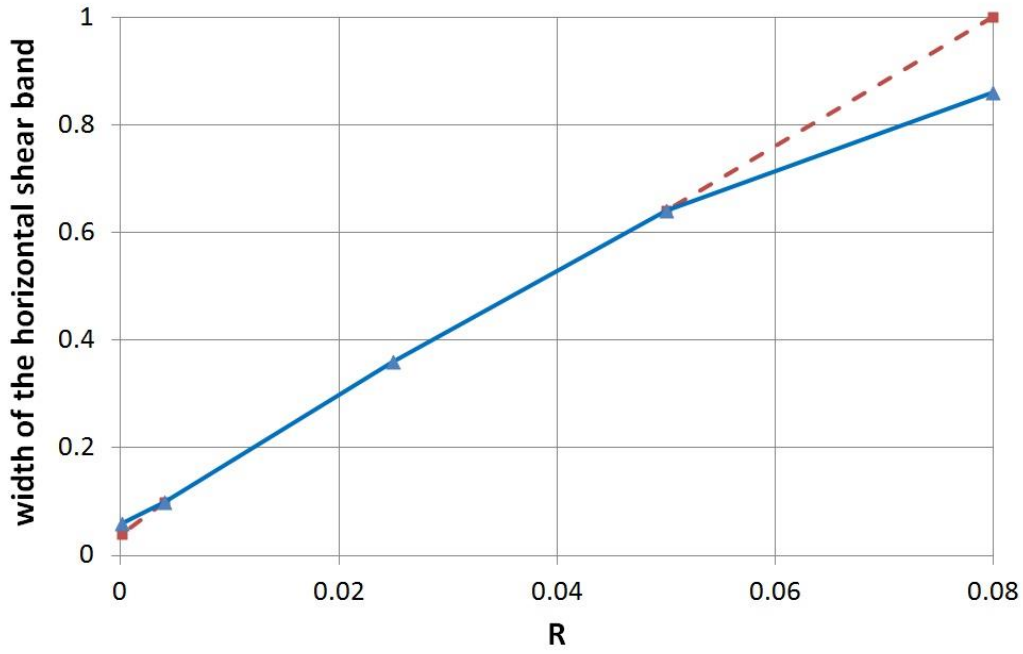

Figure 11: Representation of the width of the horizontal shear band as a function of the parameter *R*.

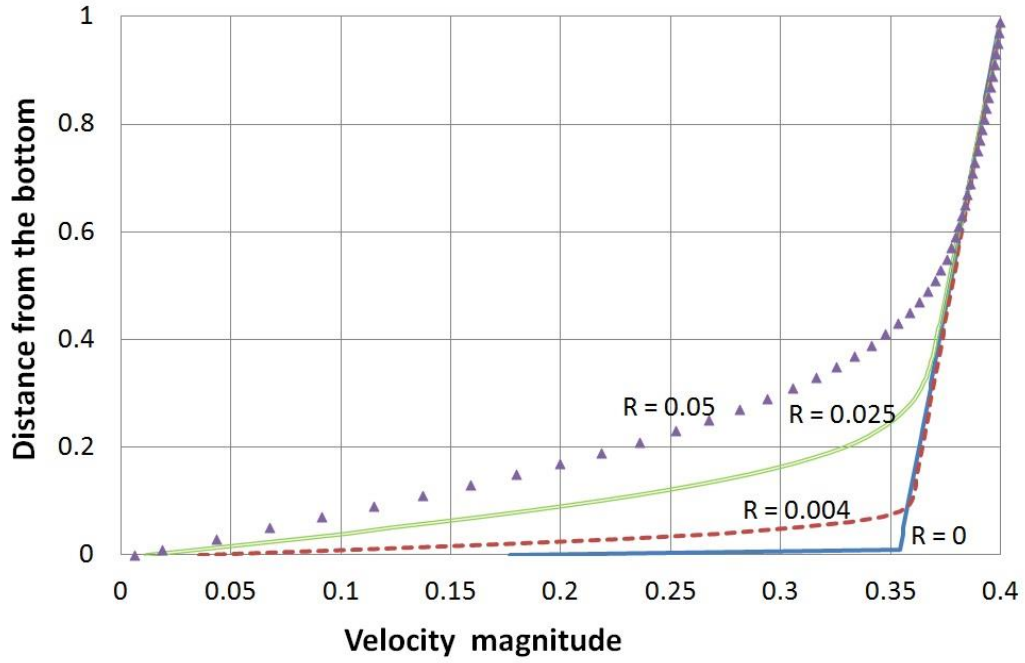

Figure 12: Final velocity profile for different values of *R*.

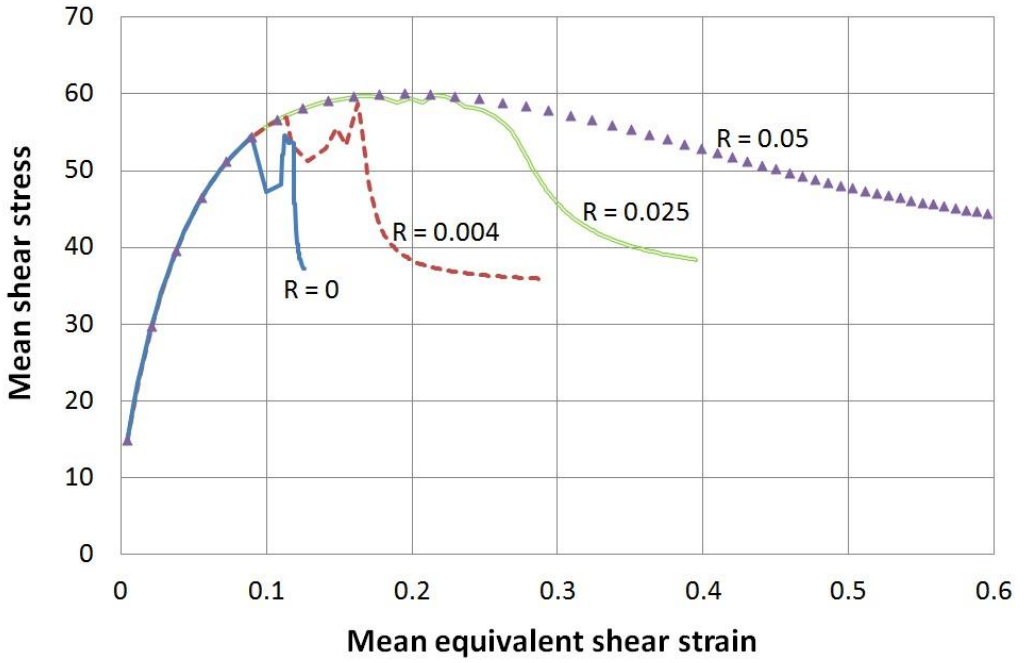

Figure 13: Stress-strain curve for different values of *R*.

Dimensions: width x height	4 x 1
Mesh (number of elements): horizontally x vertically	400 x 100
Dimensions of the weak zone: width x height	0.04 x 0.04
Coordinates of the centre of the weak zone	$x_1 = 2$; $y_1 = 0.02$
Background viscosity η	800
Background viscosity of the weak zone η_w	8
Hardening parameters	$\mu_0 = 0.1$; $\mu_\infty = 0.245$; $n = 7$
a_1 (for Cosserat only)	0.5
a_2 (for Cosserat only)	0.25
a_3 (for Cosserat only)	0.25

Table 1. Reference parameters. Note that the problem is dimensionless.